[American Journal of Science, Vol. 308, February, 2008, P. 105–129, DOI 10.2475/02.2008.01]

American Journal of Science

FEBRUARY 2008

TURBIDITE DEPOSITIONAL INFLUENCES ON THE DIAGENESIS OF BEECHER'S TRILOBITE BED AND THE HUNSRÜCK SLATE; SITES OF SOFT TISSUE PYRITIZATION

ROBERT RAISWELL*, ROBERT NEWTON*, SIMON H. BOTTRELL*, PATRICIA M. COBURN*, DEREK E. G. BRIGGS**, DAVID P. G. BOND*, and SIMON W. POULTON***

ABSTRACT. Chemical signatures of enrichment of highly reactive iron, and framboid size distributions, are reported in turbidite sediments that host soft tissue pyritization (Beecher's Trilobite Bed, Upper Ordovician, and the Hunsrück Slate, Lower Devonian). These signatures demonstrate that the sediment of Beecher's Trilobite Bed was enriched in highly reactive iron prior to turbidite transport but that no enrichment was present in the Hunsrück Slate. Turbidite transport and resedimentation altered framboid size distributions. Small diameter framboids (< 5 μm) that formed in the sediment at the pre-transport site were lost during transport due to oxidation and/or size sorting. Larger diameter framboids (~5 – 15 μm) that formed at the pre-transport site were transported without alteration. The oxidation of the original small framboid population formed highly reactive iron (oxyhydr)oxides that were reduced during post-transport suboxic diagenesis to produce porewaters rich in dissolved iron. In some turbidites a bimodal framboid population resulted where a minor population of small diameter framboids, produced by limited sulfate reduction at the post-transport site, was added to the transported large diameter population. Soft tissue pyritization in this setting was facilitated by the presence of suboxic, iron rich porewaters where dissolved sulfide formed during soft tissue decay, confining iron sulfide precipitation to the decay site.

INTRODUCTION

Beecher's Trilobite Bed (Upper Ordovician, New York State, USA) and the Hunsrück Slate (Lower Devonian, Bundenbach, Germany) are unusual in yielding extensive examples of soft tissue pyritization (see Briggs and others, 1991, 1996; Bartels and others, 1998). In both cases pyritization occurred in fine-grained turbidites (Cisne, 1973; Sutcliffe and others, 1999). Raiswell and others (1993) hypothesized that readily metabolizable soft tissue can only become pyritized when the enclosing sediment contains low concentrations of organic C (limiting sulfate reduction and thus sulfide production) but reactive iron concentrations yield high concentrations of porewater dissolved iron as a result of iron reduction. Soft tissue that is rapidly metabolized by sulfate reduction produces H_2S rapidly and high concentrations of dissolved iron are required to confine iron sulfide precipitation to the decay site. The rarity of soft tissue pyritization suggests that unusual factors are involved in creating the necessary diagenetic conditions, and the geochemical studies by Briggs and others (1991, 1996)

*School of Earth and Environment, University of Leeds, Leeds LS2 9JT, United Kingdom; raiswell@see.leeds.ac.uk

**Department of Geology and Geophysics, Yale University, P.O. Box 208109, New Haven, Connecticut 06520-8109, USA

***School of Civil Engineering and Geosciences, University of Newcastle upon Tyne, Newcastle NE1 7RU, United Kingdom

indicated that both sedimentary sequences were enriched in highly reactive iron. Turbidite deposition played a key role by burying organisms rapidly (thus preventing prolonged exposure on the seafloor) but it may also have been important in enriching the content of highly reactive iron that was easily reduced to dissolved iron.

In Phanerozoic marine sediments, enrichment in highly reactive iron usually occurs where deposition takes place below a sulfidic water column (for example, Raiswell and Anderson, 2005; Lyons and Severmann, 2006). It has been suggested that such enrichment is the result of diagenetic mobilization of iron from basin margin sediments followed by transport to the deep basin where iron can be scavenged from a sulfidic water column by pyrite formation (Wijsman and others, 2001; Raiswell and others, 2001; Lyons and others, 2003; Raiswell and Anderson, 2005; Lyons and Severmann, 2006). However both Beecher's Trilobite Bed (Cisne, 1973) and the Hunsrück Slate (Sutcliffe and others, 1999) were deposited in oxygenated bottom waters and scavenging from a sulfidic water column was therefore impossible.

Alternatively the physical processes involved in turbidite deposition may have added or removed different sediment components that influenced the content of highly reactive iron. Turbidite deposition from an oxygenated water column onto anoxic sediment, for example, produces redox discontinuities that may result in complex patterns of diagenetic iron mobilization and enrichment. Mucci and Edenborn (1992) and Delfandre and others (2002) observed the migration of iron following the rapid deposition (10–50 cm in 3 weeks) of oxic sediment onto anoxic marine sediment. Upward migration of the redox boundary into the newly added sediment released Fe^{2+} from iron oxides, and the dissolved Fe^{2+} migrated both upwards to the new sediment surface (where it precipitated as oxide) and downwards to the anoxic sediment boundary (where it precipitated as sulfide). Ultimately the iron oxide concentrated at the new sediment surface was buried and pyritized, so that both the old and the new sediment surfaces are represented by pyrite-rich layers. Similar iron-rich layers have been recorded where distal turbidites are deposited on dysoxic pelagic sediments (Wilson and others, 1985, 1986).

The complex physical processes that occur during turbidite deposition need to be considered alongside the chemical signatures in order to evaluate how deposition influences highly reactive iron content. Chemical signatures of highly reactive iron enrichment include the ratio of highly reactive iron (Fe_{HR}) to total iron (FeT), and the ratio of FeT to Al (Werne and others, 2002; Lyons and others, 2003). We analyzed these chemical signatures to determine whether iron enrichment in the Hunsrück Slate and Beecher's Trilobite Bed was a product of turbidite deposition. We also evaluated the impact of physical processes on highly reactive iron enrichment by examining framboid size distributions. Framboids are densely packed spherical aggregates of equigranular micron-sized pyrite crystals (Love and Amstutz, 1966; Rickard, 1970; Wignall and Newton, 1998; Ohfuji and Rickard, 2005). The size range of framboidal pyrite in euxinic environments is significantly smaller than in sediments deposited beneath oxic and dysoxic water columns, but both populations have log-normal size distributions (Wilkin and others, 1996, 1997). These size distributions may be modified, however, by turbidite deposition that involves either graded deposition from a waning flow, erosion (for example, Wignall and Newton, 1998), or mixing with different sediment populations (Formolo and Lyons, 2007). Thus framboid size distributions may reveal the role of physical processes.

BACKGROUND

Chemical Signatures of Reactive Iron Enrichment

Determining highly reactive iron enrichment requires the identification of a chemical signature of enrichment and a baseline for comparison. Highly reactive iron

concentrations can only be compared directly where differences in the dilution effects of non-iron bearing minerals (for example biogenic material) are small. Hence ratios such as Fe_{HR}/FeT, and FeT/Al, which correct for dilution effects, are the preferred signatures of enrichment. Enrichment of highly reactive iron is defined here as an increase in the (oxyhydr)oxide iron content (see below) relative to the aluminosilicate fraction of the sediment. Baseline data for identifying enrichments in mean ratio values (Fe_{HR}/FeT, FeT/Al) are usually derived from sediments either in the same basin (Werne and others, 2002; Lyons and others, 2003) or from the average composition of shales from geographically widespread sources. Both approaches are used here. However, both require that baseline data are derived from sediments with similar depositional environments and late diagenetic/metamorphic histories. This ideal may not be easy to achieve even when data from intra-basinal sediments are used as a baseline, but is more difficult with a geographically widespread set of sediment data.

The Fe_{HR}/FeT ratio quantifies the proportion of total iron that is highly reactive toward sulfide (and thus forms pyrite) during anoxic marine diagenesis. In anoxic marine sediments sulfate reducing bacteria oxidize organic matter generating H_2S (Berner 1970, 1984), a fraction of which reacts with detrital iron minerals to form pyrite. The initial products are usually iron monosulfide minerals, which are transformed to pyrite by reaction with polysulfides (Goldhaber and Kaplan, 1974; Rickard, 1975; Luther, 1991; Schoonen and Barnes, 1991; Hunger and Benning, 2007; Rickard and Luther, 2007).

Modern sediment studies (Canfield, 1989; Canfield and Raiswell, 1991; Canfield and others, 1992; Poulton and others, 2004) have shown that iron oxides react rapidly with dissolved sulfide, while only relatively small proportions of aluminosilicate iron react, even over time-scales of millions of years (Canfield and others, 1992; Raiswell and Canfield, 1996). Thus the concentration of iron that is highly reactive towards dissolved sulfide (Fe_{HR}) is measured as the sum of the iron that is extracted by dithionite (FeD, that is, iron present mainly as oxides with small concentrations of silicates: Raiswell and others, 1994) plus iron that has already reacted with sulfide (FeP, that is, iron present as pyrite or other sulfides). The only baseline data available for the Fe_{HR}/FeT ratio are for modern oxic shelf and deep sea sediments (Raiswell and Canfield, 1998) where the maximum value is 0.4. Raiswell and Canfield (1998) suggested that values greater than 0.4 clearly indicate enrichment. However the average Fe_{HR}/FeT ratio for these oxic sediments is 0.28 ± 0.06 and some iron enrichment therefore may be present where the Fe_{HR}/FeT ratio is below 0.4.

Unfortunately these modern data may not be applicable to ancient sediments due to the loss of Fe_{HR} with burial. Poulton and Raiswell (2002) showed that mean values of Fe_{HR}/FeT are significantly higher in modern oxic sediments (0.28 ± 0.06) than in those from Mesozoic and Paleozoic sediments (which range from 0.13 ± 0.06 to 0.17 ± 0.11). Aplin and Macquaker (1993) showed that the Ferrous/(Ferrous + Ferric) ratio of the Kimmeridge Clay (Jurassic) increases with increasing burial to depths of approximately 4 km, as ferric iron in mixed layer illite-smectite and iron oxides is reduced to ferrous iron with depth and incorporated into iron chlorite. Garrels and Mackenzie (1971) showed a similar trend in shales with increasing age, which they attributed to the reduction of oxide iron by organic C during deep burial. These observations indicate that highly reactive iron is reduced and incorporated into non-dithionite soluble minerals, so that Fe_{HR}/FeT decreases with increasing burial and/or age (Poulton and Raiswell, 2002). These changes in Fe_{HR}/FeT demonstrate the importance of deriving baseline data from sediments of a similar age and burial history in order to constrain the effects of late diagenetic/metamorphic changes on Fe_{HR}/FeT ratios.

Highly reactive iron enrichment is also revealed by high values of the FeT/Al ratio (Werne and others, 2002; Lyons and others, 2003), which are less affected by late

diagenesis/metamorphism (see below). Highly reactive iron is closely associated with aluminosilicates (for example, Poulton and Raiswell, 2005) and enrichment in Fe_{HR} produces a corresponding increase in FeT. Normalizing FeT to Al minimizes dilution effects arising from variations in the aluminosililicate fraction (see above). Baseline data are commonly derived from values of FeT/Al in average shale and these show no consistent changes with burial depth and/or temperature (for example, Garrels and Mackenzie, 1971). The FeT/Al ratio of average shale ranges from 0.5 to 0.56 (Clarke, 1924; Ronov and Migdisov, 1971; Taylor and McLennan, 1985) but these values are based on data from both oxic and euxinic sediments (the latter possibly Fe-enriched with relatively high FeT/Al values).

Baseline sediment data are derived here by using mean ratio values and measures of uncertainty for: 1. Beecher's Trilobite Bed and Hunsrück Slate sediments that are lithologically and stratigraphically closely associated with the sediments that yield pyritized soft tissue; and 2. a geographically widespread suite of Paleozoic sediments from oxic marine environments (see Raiswell and Berner, 1986).

Note that the Fe_{HR}/FeT and FeT/Al ratios record somewhat different enrichment signatures (Anderson and Raiswell, 2004). The Fe_{HR}/FeT ratio records enrichment arising from both the addition of Fe_{HR} and the formation of Fe_{HR} from other forms of less reactive lithogenous iron, whereas the FeT/Al ratio records reactive iron enrichment resulting only from the addition of Fe_{HR} to the sediment. Thus a comparison of both ratios may allow the effects of addition to be distinguished from enhancement of reactivity.

Framboid Size Distributions

A variety of theories have been proposed to explain the microstructure of framboids (see Ohfuji and Rickard, 2005). Their sphericity has been interpreted as inherited from microbial cells (Massad, 1974), amorphous iron monosulfide gels or globules (Love and Amstutz, 1966; Sawlowicz, 1993), humic globules (Papunen, 1966), or gas vacuoles (Graham and Ohmoto, 1994), or resulting from magnetic aggregation (Wilkin and Barnes, 1997). The organization of the microcrysts has not yet been explained although it may reflect the interplay of attractive and repulsive forces in iron monosulfide suspensions (Wilkin and Barnes, 1997) where a high supersaturation of pyrite produces a high nucleation density (Ohfuji and Rickard, 2005).

Ohfuji and Rickard (2005) showed that the experimental formation of framboids requires an extremely high supersaturation of pyrite, which can be achieved by the addition of polysulfides or oxygen. Polysulfides are also necessary for pyrite formation from precursor iron monosulfides (Hunger and Benning, 2007). In natural systems oxygen, even in trace concentrations, plays a critical role by increasing the redox potential and thus the degree of supersaturation. Polysulfides also are supplied readily to anoxic sediments, directly or indirectly, by the addition of dissolved oxygen from bioturbation and bioirrigation (where the overlying waters are oxic or dysoxic). In euxinic sediments, however, polysulfides are available only at the redox boundary in the water column (Wilkin and others, 1996, 1997). Sulfur isotope measurements on sediment trap material and on water column dissolved sulfide have confirmed that framboids form at the redox boundary within the water column of the Black Sea (for example, Muramoto and others, 1991; Calvert and others, 1996; Lyons, 1997; Wilkin and Arthur, 2001).

The size distribution of framboids formed at the redox interface in euxinic water columns is probably limited by a variety of factors that control their buoyancy (Wilkin and others, 1996, 1997). Framboids that settle from the water column into euxinic sediments cannot continue to grow (and no new framboids can form) because oxygen is unavailable, although infilling and overgrowth may occur through the direct precipitation of pyrite at low degrees of supersaturation. In contrast framboids can continue to grow in sediments deposited from oxic and dysoxic bottom waters due to

the availability of oxygen. The different size distributions of framboids in euxinic and oxic/dysoxic sediments provides a basis for their use as a paleoredox indicator (Wilkin and others, 1996; Wignall and Newton, 1998). In both cases the framboid size distributions are log-normal (Wilkin and others, 1996, 1997) and plots of mean framboid size against the standard deviation of the mean size clearly distinguish oxic/dysoxic sediments from euxinic sediments. However turbidite deposition is likely to produce deviations from log-normal where framboid size fractions are lost or concentrated, or mixed with different populations eroded from substrate sediments. The influence of turbidite deposition on framboid size distributions has not been documented.

DEPOSITIONAL SETTING

Beecher's Trilobite Bed

Beecher's Trilobite Bed (BTB) is a layer of dark gray mudstone approximately 4 cm thick within the Frankfort Shale in upper New York State, USA (Cisne, 1973). The base of BTB is a coarse silt separated from an underlying graptolitic shale by an erosive contact. The graptolitic shale accumulated during slow sedimentation and includes much biogenic debris (Cisne, 1973; Briggs and others, 1991). The basal silt grades upwards rapidly into a horizon with ripple marks, above which the bed is dominated by clay with ~5 percent of larger clasts of organic matter and pyrite. Beecher's Trilobite Bed (BTB) is a classic horizon for the three dimensional pyritization of trilobite soft tissue. Trilobites with pyritized limbs are concentrated through an interval of only a few millimeters. The BTB represents a single influx of sediment that resulted in a mass mortality.

The microstratigraphy of BTB was described by Cisne (1973, fig. 2) and a detailed log of a 30 cm sequence of Frankfort Shale including the bed was presented by Briggs and others (1991, fig. 2). This sequence consists of thin beds of fine sand and silt turbidites interbedded with thin beds of black graptolitic shale (Briggs and others, 1991, fig. 2). The BTB and associated sediments preserve sole markings and internal structures indicating a turbidite origin. While there is a reasonable diversity of taxa within the BTB (Cisne, 1973) the assemblage is dominated by the trilobite *Triarthrus eatoni* which belongs to the Olenidae, a family that Fortey (2000) argued was tolerant of low oxygen or, sulfide-rich environments and may have included chemoautotrophic symbionts. The sedimentary structures, combined with the preservation of delicate features in the fossils and their lack of sorting, suggest that the organisms were not transported far (Cisne, 1973).

The Hunsrück Slate

The Lower Devonian Hunsrück Slate (HS) is under investigation as part of *Project Nahecaris* (Bartels and others, 2002a), which has yielded data on the nature and distribution of sedimentary facies (Sutcliffe and others, 1999, 2002) that provide a valuable context for the present study. The pyritized fossil bearing beds occur in a ~65 m thick coarsening upward sequence formed by the progradation of a fan into a shelf setting, as evidenced by interbedded sandstones and claystones with coquinas. The fossils were deposited by low velocity density currents in low lying areas of the seafloor (depths just below storm wave-base) in lower fan or inter-channel deposits. The main lithology is dark laminated slate with interbedded sand, silt and clay (Sutcliffe and others, 1999, 2002). Significant examples of soft tissue pyritization in the HS are restricted to four thin roof slate horizons (Bartels and others, 1998, fig. 16; Sutcliffe and others, 1999, fig. 2) but it is not known whether or not pyritized fossils were confined to a single event at each of these horizons. Pyritized fossils are extremely rare and tons of slate may be worked without finding a single specimen (Bartels and Brassel, 1990; Briggs and others, 1991).

The microstratigraphy of a 6 m excavated section in the Eschenbach Member of the Hunsrück Slate was illustrated by Sutcliffe and others (2002). Ichnological and sedimentological studies of the HS (Brett and Seilacher, 1991; Sutcliffe and others, 1999, 2002) showed that deposition occurred as fine-grained graded turbidites as evidenced by grading and characteristic sedimentary structures including flute casts and tool marks. Brett and Seilacher (1991) interpreted the sediments as obrution deposits formed below storm wave base under a stratified, dysoxic water column, but Sutcliffe and others (1999) showed that the water column was well oxygenated. The animals (mainly echinoderms and arthropods: Bartels and others, 1998, 2002b) were alive during entrainment and deposition and escape structures indicate that not all organisms were entombed (Sutcliffe and others, 1999); some were buried *in situ*. The taxa in these event horizons are similar to those in the overlying and underlying beds (Bartels and Brassel, 1990; Bartels and others, 2002b). Tibbs (ms, 2001) and Sutcliffe and others (2002) noted that the pyritized fossil-bearing beds are more sandy and light gray in color (silt-prone), whereas the sediments without soft-bodied fossils are finer-grained and darker (clay-prone). Beds of both these facies range up to 5 cm in thickness, in contrast to the much thinner samples containing pyritized fossils analyzed here. The sediment enveloping the pyritized fossils is also characterized by thin sedimentary laminae, a low abundance of infauna and weak bioturbation, indicating that conditions within the sediment were generally anoxic and inhospitable. Calcareous shells (molluscs and brachiopods) are commonly dissolved out of the HS in the area around Bundenbach (Bartels and others, 1998).

SAMPLING AND ANALYTICAL METHODOLOGY

Samples from BTB were available from a previous study (Briggs and others, 1991, 1996) and additional analytical data were derived for the chemical signatures used here. A sequence including the main Trilobite Bed was collected by removing material from a freshly-exposed surface and cutting a continuous sequence of blocks (Briggs and Edgecombe, 1993). This provided a series of 8 samples at one centimeter intervals from ~6 cm below to ~6 cm above BTB (see Briggs and others, 1991, fig. 2), which are termed the host sediment suite. Five samples of the Trilobite Bed associated with pyritized fossils were used to define a pyritiferous turbidite suite that allowed an intra-basinal comparison with the host sediment suite. Framboid size measurements were made on four samples: two samples of the Trilobite Bed associated with pyritized fossils (B/103 and B/109), one sample of the graptolitic shale (B1) below the BTB and one sample of the silty turbidite (B2) at the base of the Trilobite Bed above the erosive contact with B1.

HS samples used in a previous study (Briggs and others, 1996) were re-analyzed during the present investigation to determine their chemical signatures. A suite of 23 samples (hereafter termed the pyritiferous turbidites) were available from Eschenbach-Bocksberg quarry within slate at varying distances from the edges of pyritized fossils. These samples were collected by splitting loose blocks in the quarry, and their stratigraphic postion and orientation are unknown. Two new samples were collected from the slate surrounding pyritized fossils; a gastropod (H/G) and a specimen of the asteroid *Furcaster* (H/F). These samples were also analyzed and the data incorporated into the pyritized turbidite suite. None of the samples contained vein sulfides or coarse-grained pyrite. A further 10 samples of sediment containing unpyritized fossils (Briggs and others, 1996; Appendix 2) were analyzed from a variety of HS localities where pyritization does not occur (the non-pyritiferous turbidites). Finally 11 samples were analyzed from a sediment block (about 15 cm thick) that includes a lens of pyrite but no recognizable fossil material (the host turbidites). The thickness of these samples of host turbidites, and their position within the block, is illustrated in Briggs and others (1996, fig. 6). The pyritiferous turbidites were contrasted with the non-

TABLE 1

Paleozoic sediment samples and their mean FeT/Al, Fe_{HR}/FeT and Fe_{PR}/FeT (for further details see Raiswell and Berner, 1986)

Age	Sample Description	No. of Samples
Lower Ordovician	Tattenhoe borehole, UK	22
	Deanshanger borehole, UK	1
	Lillingstone Lovell borehole, UK	1
Middle and Upper Ordovician	Oslo, Norway	9
	Ohio-Kentucky, USA	11
	Cautley Formation, UK	6
	Snake Hill Shale, USA	13
	Great Paxton borehole, UK	3
Silurian	Cautley Formation, UK	3
	Ohio-Kentucky, USA	3

Composition	Mean Paleozoic Shale
No. of samples	72
% Fe_{HR}	0.69±0.56
%Fe_{PR}	1.80±0.85
% FeT	4.59±1.31
% Al	8.68±2.94
Fe_{HR}/FeT	0.15±0.10
Fe_{PR}/FeT	0.39±0.11
FeT/Al	0.53±0.11

pyritiferous turbidites and the host turbidites to provide an intra-basinal comparison. Framboid size measurements were made on four of the above samples; two of the pyritiferous turbidites (H/G and H/F) and two of the host turbidites (H1 and H2).

A Paleozoic iron speciation database was constructed using 72 samples (from Raiswell and Berner, 1986) deposited under an oxygenated water column, for which new total element and iron speciation data were obtained (table 1). Pyrite formation in these sediments was limited by the concentrations of highly reactive iron (Berner, 1984; Canfield and others, 1992; Raiswell and Canfield, 1998). Iron enrichment by diagenetic recycling is unlikely to have occurred in the absence of a sulfidic water column. The database contains sediments from a wide variety of depositional environments with varying proportions of aluminosilicate minerals (and thus Fe_{HR} contents),

which are expressed in terms of the ratios Fe_{HR}/FeT and FeT/Al. These Paleozoic samples provide satisfactory baseline data for comparisons of reactive iron contents in turbidites that may have mixed shelf and basin/slope characteristics. Iron speciation data for the Paleozoic samples, plus the samples from BTB and the HS, were analyzed with an extraction scheme that yields three fractions commonly used to define the reactivity of sediment iron towards dissolved sulfide. Amorphous and crystalline iron oxides (with the exception of magnetite) were solubilized by a citrate-buffered (pH = 4.8) sodium dithionite solution (Canfield, 1989; Raiswell and others, 1994). The same oxides, together with iron present as magnetite and some silicate iron, were extracted using boiling 12N HCl (Berner, 1970; Raiswell and others, 1994). All dissolved iron analyses were measured by flame AAS. Total iron and Al were measured by XRF following a lithium borate fusion. Measurements on replicate samples indicate a precision of < 4 percent for all methods.

The iron extracted by dithionite (FeD) from oxides is considered to be highly-reactive towards dissolved sulfide and may be converted to pyrite following deposition in the marine environment (see earlier). Thus the highly reactive iron content (Fe_{HR}) of marine sediments includes iron present as oxides (FeD) plus that present as pyrite and acid volatile sulfides (FeP); Fe_{HR} = FeD + FeP. Like dithionite, boiling HCl removes iron (FeH) that is present as oxides, but it also removes iron in poorly reactive silicates that is only sulfidized on a time scale of 10^5 to 10^6 years (Canfield and others, 1992; Raiswell and Canfield, 1996). Hence FeH-FeD represents an iron fraction that reacts only slowly with dissolved sulfide and here is termed poorly reactive (Fe_{PR}).

The determination of mean element ratios and their errors is not straightforward (see Raiswell and Berner, 1986). Values derived from regression plots of concentration data exaggerate the influence of samples with high concentrations, and average ratio values exaggerate the influence of extremes that result when either concentration is relatively low. Furthermore distributions of the ratios Fe_{HR}/FeT, Fe_{PR}/FeT and FeT/Al in the Paleozoic sediment database vary from normal towards log-normal. The ratio $(Fe_{HR)av}/(FeT)_{av}$ provides a good estimate (with a bias of approximately 1/n) for the mean of a set of n values of Fe_{HR}/FeT, where the exact distribution of Fe_{HR}/FeT is unknown (Koch and Link, 1971). This approach was followed for the Paleozoic database. However, in the case of the smaller databases of BTB and HS, ratio values derived in this way were essentially the same as the mean values of the individual ratios. Tests of the Fe_{HR}/FeT and FeT/Al data indicate that the deviations from normal are not large. Thus standard deviations of these ratios can be used as a measure of uncertainty which can be evaluated by a Student's t test. The Fe_{PR}/FeT data deviate substantially from normal; standard deviations of this ratio were calculated for completeness but were interpreted cautiously. Only differences at the < 1 percent level are considered to be significant unless otherwise stated.

Framboid sizes were measured on polished blocks and thin sections using BSE imaging on a Camscan Series 4 scanning electron microscope (operated with a 20 kV beam, 1 nA sample current, at an image distance of 20 mm). Ohfuji and Rickard (2005) defined framboids as spheroidal/sub-spheroidal clusters of equidimensional and equimorphic microcrystalline pyrite crystals. These characteristics are recognizable even when framboids are overgrown by later phases of pyrite (figs. 1A and 1C). Size measurements were made to $\pm$ 0.5 μm directly from the SEM screen. Such sections through spherical grains tend to underestimate the true diameter but Wilkin and others (1996) showed that this effect is small ($< 10\%$ of mean diameter). Each sample produced more than 90 measurements of type 1 framboids (as defined above). Larger, more loosely packed and partially compacted aggregates (type 2 framboids of Wignall and Newton, 1998) are excluded from the above definition and were not considered.

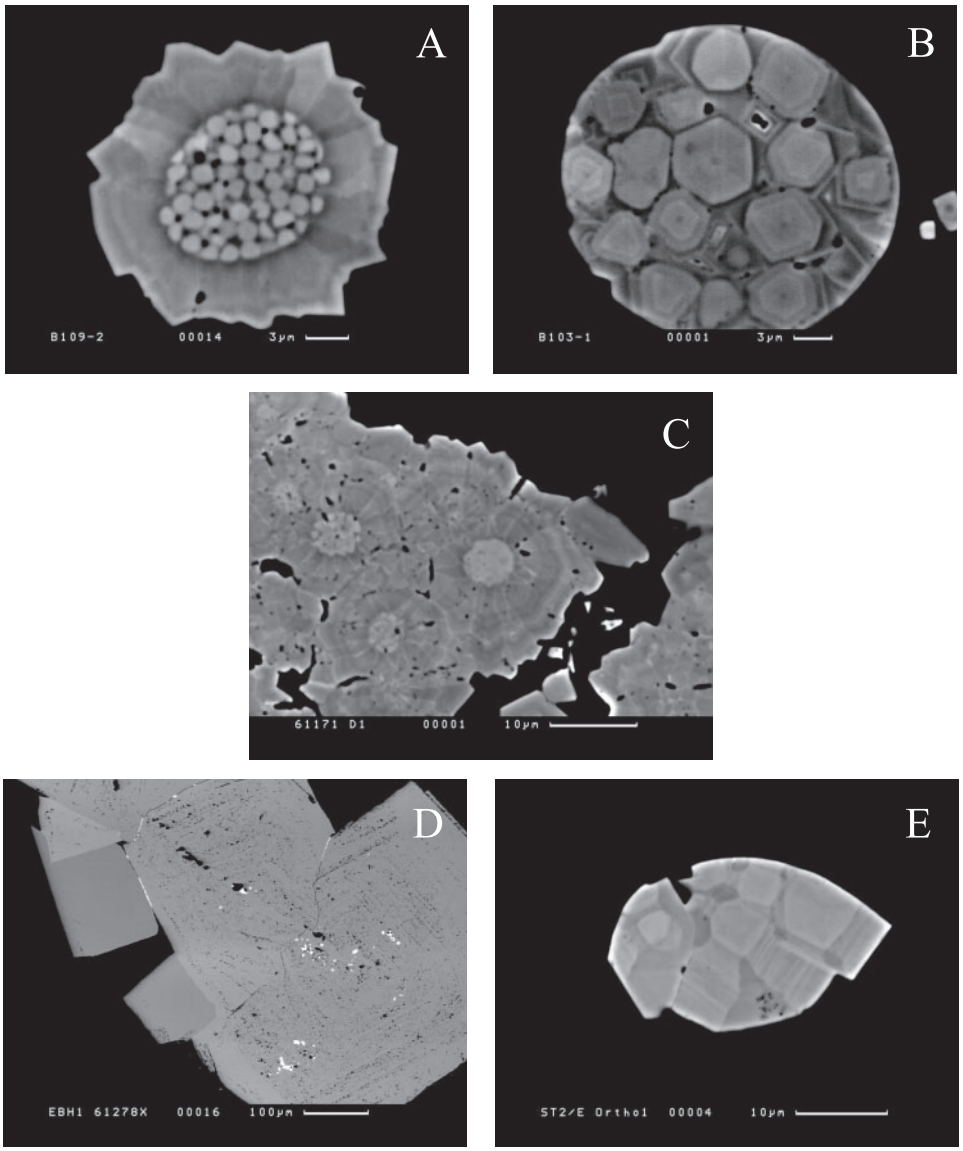

Fig. 1. Pyrite morphologies. (A) Beecher's Trilobite Bed. Pyritiferous turbidite showing framboidal pyrite enveloped by euhedral pyrite with light and dark growth zones. (B) Beecher's Trilobite Bed. Pyritiferous turbidite showing an aggregate composed of euhedral pyrite with rounded erosive margins that crosscut growth zones. (C) Hunsrück Slate. Host turbidites showing framboidal pyrite enveloped by euhedral pyrite with light and dark growth zones. (D) Hunsrück Slate. Host turbidites showing coarse-grained idioblastic pyrite formed during metamorphism. (E) Hunsrück Slate. Pyritiferous turbidites showing an aggregate composed of euhedral pyrite with growth zones truncated by erosion.

The framboid size distributions in BTB and the HS were examined to assess the influence of turbidite depositional processes and their effect on the paleoredox plots of mean framboid size against standard deviation. Framboid size distributions typically show log-normal distributions (Wilkin and others, 1996, 1997) which produce straight lines on a plot of log (framboid diameter) against probability (expressed as cumulative

percent). Sinclair (1974) distinguished unimodal log-normal data, which plot as a straight line, from bimodal distributions, which plot as a curve (where there is a considerable overlap of the two populations) or as two intersecting straight lines (where the population overlap is small).

The paleoredox plots of Wilkin and others (1996) are based on relatively few ancient sediment data and so we compiled a database of framboid size distributions from Wignall and Newton (1998), Newton (2001), Coburn (2003) and Bond (ms, 2004) for 104 ancient sediments ranging in age from the Devonian to the Jurassic (table 2) to assist in examining the relationship of framboid size distributions to bottom water oxygenation. The depositional paleoredox environments of these ancient sediments were defined according to the Oxygen-Restricted Biofacies (ORB) scheme (Wignall and Hallam, 1991; Wignall, 1994), based on observations of benthic species diversity and sediment fabric. Two anaerobic biofacies (ORB 1 and 2) are defined by the complete absence of benthic metazoans but they differ in that ORB 1 contains only truly pelagic taxa whereas ORB 2 also contains taxa regarded as nektobenthic (implying the absence of a significant layer of sulfidic bottom water). Wignall and Newton (1998) found that both anaerobic ORBs yielded similar framboid size distributions but that rare large framboids formed in ORB 2 during brief periods of oxygenation. ORB 3 and 4 contain impoverished benthic assemblages, which are resticted to a few bedding planes in sediments that are otherwise laminated and lack bioturbation, indicating that oxygen was available only transiently in the bottom waters (that is, lower dysaerobic facies). ORB 1 to 4 here are classified as anoxic, as subtle differences in the extent of bottom water oxygenation are not our focus. Upper dysaerobic biofacies (ORB 5 and 6) are characterized by increases in benthic species and were probably persistently dysoxic, in contrast to the intermittent oxygenation of ORB 3 and 4. ORB 5 to 6 differ from sediments deposited from oxic (that is, fully oxygenated) bottom waters, which show greater benthic diversity including stenoxic taxa such as thick-shelled and burrowing forms (Wignall and Newton, 1998). Samples from ORB 4.5–6 plus oxic samples are used to define an oxic/dysoxic sample suite for the paleoredox plots.

RESULTS

Petrography

The BTB is a mudstone which contains pyrite framboids that may be isolated or overgrown by euhedral pyrite (fig. 1A). Framboids are often concentrated in remnant organic matter, but no pyrite-rich laminae were observed. Euhedral pyrite often shows growth zones and may be assembled in complex aggregates, the margins of which are smooth and crosscut growth zones (fig. 1B), indicating abrasion during turbidite transport. No abrasion effects were evident in framboids that were not enveloped in euhedral pyrite, possibly because of their sphericity. The underlying thin graptolitic shale contains abundant framboids.

The HS is a slate consisting mainly of chlorite, muscovite (phengite) and quartz with diagenetic pyrite, ankerite and apatite. Chlorite-muscovite porphyroblasts formed during low grade metamorphism, silica was re-mobilized and three stages of cleavage developed (Talbot, 1964; Roy, 1978; Bartels and others, 1998; Wagner and Boyce, 2006). Late stage fractures developed at this time and were infilled by quartz and sulfides. Metamorphic sulfides occur at the contacts between early diagenetic pyrite and the slate matrix (Wagner and Boyce, 2006). Diagenetic pyrite is fine-grained (typically < 20 μm) and occurs as single crystals, framboids and euhedral masses. Framboids occur as isolated grains, concentrated in remnant organic material (in some cases fish coprolites: Wagner and Boyce, 2006), or enveloped in euhedral masses that often show light and dark growth zones (fig. 1C). Framboids enveloped in

TABLE 2

Framboid size distributions from Wignall and Newton (1998), Newton (2001), Coburn (2003) and Bond (2004)

SECTION	ORB	NUMBER OF FRAMBOIDS	MEAN	SD	MIN. SIZE m
Gray Shales, Early Jurassic, Yorkshire, UK					
KN-15	2	275	5.60	2.59	1.5
BW-16a	2	231	4.72	2.08	1.5
BW-32b	2	208	4.80	2.21	1.5
Jet Rock, Early Jurassic, Yorkshire, UK					
RB-2b	2	224	4.57	1.98	1.5
RB-2b/i	2	261	4.86	2.44	1.5
Williston Lake, Permo-Triassic, BC, Canada					
UC-28	2	100	5.76	2.31	2.5
UC-43	1	150	6.04	2.58	2
Kimmeridge Clay, Late Jurassic, Dorset, UK					
White Stone Band	1	192	3.10	1.11	1
W-17	1	175	3.57	1.18	1.5
W-36	1	129	3.79	1.25	1.5
Devils Gate, Late Devonian, Eureka Co., Nevada, USA					
Devils Gate Bed 4	1/2	90	5.54	2.01	2.5
DG Bed 7 (middle)	1/2	103	3.77	1.24	1
DG Bed 26	1/2	95	5.08	1.43	2.5
DG Bed 29 (middle) (UKH)	1/2	114	4.40	1.69	2
Coyote Knolls, Late Devonian, Utah, USA					
Bed 9	1/2	110	4.26	1.41	1.5
Bed 17	1/2	104	5.43	2.58	2.5
Bed 19	1/2	95	5.29	1.96	2.5
Bed 22	1/2	103	4.76	1.62	1.5
Bed 29	1/2	106	3.66	1.30	1.5
Bed 30	1/2	99	4.28	2.00	1.5
Steinbuch Benner, Late Devonian, Germany					
B22 - Bed 28 (LKH)	1/2	127	4.74	1.59	2
B35 - Bed 44 (UKH)	1/2	131	4.73	2.05	1.5
B36 - Bed 45 (UKH)	1/2	136	4.21	1.66	1.5
B38 - Bed 47	1/2	132	6.24	2.42	1.5
Kowala, Late Devonian, Poland					
KQ 22 - Kowala	1/2	105	5.00	1.75	2
KQ 63 - Kowala	1/2	131	4.38	1.77	1
La Serre, late Devonian, Cabrieres, France					
C - 14b	1/2	130	4.86	1.71	2
C - 14f	1/2	129	4.76	1.87	1.6
C - 15b	1/2	125	4.72	1.84	2
C - 9	1/2	126	4.47	1.56	1.5
C - 14a	1/2	142	4.78	1.66	2
White Rock Canyon, Late Devonian, Nevada, USA					
WRC bed 3 (middle)	1/2	95	4.46	2.13	2
WRC bed 4 (top)	1/2	98	4.23	1.55	2
WRC bed 6 (top)	1/2	100	5.49	1.95	2
WRC bed 10 (top)	1/2	106	4.79	1.68	2

TABLE 2
(continued)

SECTION	ORB	NUMBER OF FRAMBOIDS	MEAN	SD	MIN. SIZE μm
Black Bear Ridge, Late Devonian, Willston Lake, BC, Canada					
BBR-50	4	144	4.23	1.30	1.5
BBR-21	4	134	3.99	1.30	1.5
BBR-21	4	141	4.20	1.40	2
BBR-25	4	139	4.81	1.95	1
BBR-27	4	130	4.07	1.58	1.5
BBR-28	3	126	3.90	1.32	1.5
BBR-29c	4	107	4.69	1.54	2
BBR-32	4	139	4.01	1.53	1.5
BBR-33	4	109	3.88	1.46	1
BBR-33	4	118	4.31	1.56	1.5
BBR-35	3	143	4.27	1.69	1
BBR-38	3	143	4.57	1.69	1.5
BBR-40	3	164	4.57	2.03	1.5
BBR-42	4	103	4.28	1.61	1.5
BBR-44	4	108	4.62	1.64	2
Gray Shales, Early Jurassic, Yorkshire, UK					
KN-32	4	237	5.46	2.50	1
KN-33a	4	243	5.55	2.18	1.5
BW-14b	3	275	4.69	2.00	1.5
NSB-19 (MSB-i)	3	245	4.64	2.09	1
NSB-45a	4	250	4.42	2.05	1.5
NSB-45c	4	277	4.65	1.85	1.5
NSB-45e	3	291	3.77	1.49	1
Jet Rock, Early Jurassic, Yorkshire, UK					
RB-2e	3	239	4.32	1.83	1
RB-2h	3	257	4.09	1.82	1
RB-4c	3	189	4.01	1.39	1.5
RB-4e	3	261	4.16	1.48	1.5
RB-5a	3	221	4.07	1.51	1.5
RB-7a	3	259	4.60	2.07	1.5
Permo-Triassic, Australia					
1980.85m	4	138	5.11	2.28	1.5
1978.15m	4	229	4.55	1.80	1.5
1976.55m	4	152	5.05	2.29	2
1974.85m	4	167	5.64	5.68	1.5
1969.55m (A+B)	4	322	5.37	2.43	1.5
Kimmeridge Clay, Late Jurassic, Dorset, UK					
KC/36f-1	4	136	3.31	1.48	1
KC/39a-4	3	145	4.56	1.63	1.5
KC/39c-1	3	280	3.53	1.33	1
KC/40a-1	3	206	3.46	1.68	1
KC/CS-6 (36c-2/d-1)	3	171	2.70	1.43	1
KC/CS-10 (36d-1)	4	108	3.09	1.64	1
KC/CS-12 (36d-1)	4	157	3.62	1.82	1
KC/By42d-5.8	3	134	3.05	1.08	1
Kimmeridge Clay, Late Jurassic, Boulonnais, France					
12/5/97-o	4	157	4.98	2.47	1.5
12/5/97-h	4	121	3.95	1.82	1
12/5/97-L	4	109	4.61	2.21	1.5
13/5/97-a	4	119	4.54	2.46	1.5
13/5/97-b	4	118	4.75	2.15	1.5

TABLE 2
(continued)

SECTION	ORB	NUMBER OF FRAMBOIDS	MEAN	SD	MIN. SIZE μm
Gray Shales, Early Jurassic, Yorkshire, UK					
KN-9	ox	159	6.95	3.12	2
KN-14b	ox	170	7.20	2.87	2.5
KN-19	6	128	7.21	4.03	2.5
KN-29	5	124	6.17	2.15	2
KN-31b	6	140	6.37	2.19	2
Kimmeridge Clay, Late Jurassic, Dorset, UK					
KC/cWSB-43	5	192	4.26	2.46	1.5
KC/W-4	4.5	176	4.31	2.03	2
W-7	4.5	140	5.06	2.44	2
KC/39c-2	4.5	145	3.72	1.32	1.5
KC/39c-3	4.5	88	5.92	3.08	2
KC/39d-2	5	99	7.53	4.15	2.5
KC/40a-3	5	97	6.22	3.85	2
KC/40b-1	5	116	5.88	2.76	2.5
KC/40b-2	4.5	179	5.11	2.22	1.5
KC/CS-5 (36c-2)	5	91	5.92	3.31	1.5
Kimmeridge Clay, Late Jurassic, Boulonnais, France					
12/5/97-m	6	145	5.26	3.33	2
Permo-Triassic, Australia					
1991.0m	6	121	5.79	2.84	2
1989.0m	5	123	5.65	2.23	1.5
1986.6m	5	113	4.77	1.56	2
1984.55m	6	136	5.53	1.81	1.5
1982.55m	6	120	6.08	1.99	2
1981.15m (A+B)	6	207	6.27	2.08	1.5
1972.1m	5	138	5.90	1.97	1.5

ox = fully oxygenated.

euhedral pyrite retain their distinctive characteristics and can still be used for size measurements. Metamorphic pyrite is typically coarse-grained and idioblastic (fig. 1D), and is believed to have grown partly by the dissolution-reprecipitation of early diagenetic pyrite (Wagner and Boyce, 2006).

The influence of hydrodynamic factors on framboid populations is evidenced by grading and the concentration of uniformly-sized framboids into lenses or layers that are not associated with organic structures and are presumably the product of reworking (see Wignall and Newton, 1998). Aggregate grains of pyrite occur in which erosion crosscuts individual pyrite euhedra (fig. 1E) but no abrasion effects are evident in framboids (see above). Ankerite shows no evidence of transport and usually occurs as an overgrowth on pyrite that has developed in remnant organic structures. Some ankerite crystals have dolomitic cores. SEM observations show that all these diagenetic phases developed before chlorite and re-mobilized quartz.

Chemical Signatures

The data for the Paleozoic sediments are listed in table 1. Table 3 shows the original data for BTB and the HS (Briggs and others, 1991, 1996) augmented by new samples and data for Al (not analyzed previously). Briggs and others (1991, 1996) considered Fe behavior in terms of the species extractable by dithionite (FeD) and HCl

TABLE 3

Chemical data for Beecher's Trilobite Bed and the Hunsrück Slate

Beecher's Trilobite Bed

Data	Host sediments	Pyritiferous turbidites
No. of samples	8	5
% Fe_{HR}	1.11±0.19	1.20±0.24
% Fe_{PR}	2.08±0.38	2.71±0.47
% FeT	5.26±0.24	5.43±0.17
% Al	8.60±1.33	9.17±0.18
Fe_{HR}/FeT	0.21±0.03	0.22±0.04
Fe_{PR}/FeT	0.40±0.07	0.50±0.10
FeT/Al	0.61±0.04	0.59±0.03

Hunsrück Slate

Data	Pyritiferous turbidites	Non-pyritiferous turbidites	Host turbidites
No. of samples	25	10	11
% Fe_{HR}	0.26±0.10	0.43±0.09	0.20±0.08
% Fe_{PR}	2.02±0.86	1.37±0.31	0.88±0.36
% FeT	5.61±0.38	5.07±0.32	5.43±0.20
% Al	10.2±1.07	9.58±0.82	8.90±0.81
Fe_{HR}/FeT	0.04±0.02	0.08±0.02	0.04±0.02
Fe_{PR}/FeT	0.35±0.15	0.27±0.07	0.16±0.07
FeT/Al	0.55±0.05	0.53±0.03	0.50±0.05

(FeH). This approach revealed the *post-diagenetic* composition but the *depositional* composition is revealed by quantifying the consumption of oxides to form pyrite (Fe_{HR} = FeP + FeD; see earlier) and by separating this highly reactive iron from the poorly reactive iron in HCl-soluble silicates (Fe_{PR} = FeH – FeD; see earlier). Hence the Fe analytical data in tables 1 and 3 are presented in terms of $Fe_{HR,}$ Fe_{PR} and FeT and discussed mainly in terms of the chemical signatures Fe_{HR}/FeT and FeT/Al.

The data presented here for BTB are consistent with those of Briggs and others (1991, 1996) in that the pyritiferous turbidites appear relatively high in Fe_{HR} and FeT compared to the host sediments. However these differences are not significant, nor are there significant differences in the Fe_{HR}/FeT and FeT/Al ratios. Thus the intra-basinal comparison reveals that the chemical signature of the pyritiferous turbidites is the same as that of the host sediments. Comparison with the Paleozoic sediment database, however, shows that both the pyritized turbidites and the host sediments have significantly higher values of Fe_{HR}/FeT and possibly FeT/Al (but only at the 10% level).

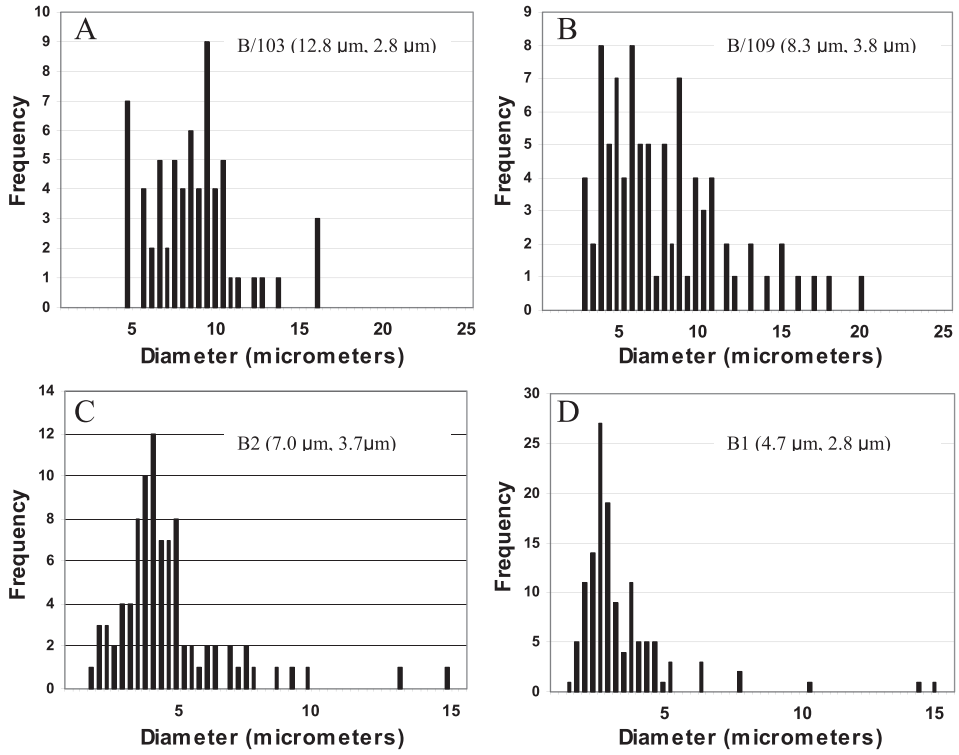

Fig. 2. Framboid size distributions in Beecher's Trilobite Bed and host sediments. (A) Pyritiferous turbidite B/103. (B) Pyritiferous turbidite. B/109. (C) Pyritiferous turbidite B2. (D) Host sediment B1.

Briggs and others (1996) noted that the pyritiferous turbidites of the HS (that is, those yielding soft-bodied fossils) are enriched significantly in FeT, FeD and FeH compared to other HS samples. Table 3 records similar enrichments in FeT and Fe_{PR} but not Fe_{HR}. The ratio data of the pyritized turbidites show similar behavior: the Fe_{PR}/FeT ratio is significantly higher than in the non-pyritiferous turbidites (at the 10% level) and the host turbidites (at the 0.1% level) but there are no significant differences in the Fe_{HR}/FeT and FeT/Al ratios. Thus the intra-basinal comparison reveals no significant differences in the main chemical signatures of the HS turbidites. Comparisons with the Paleozoic database show no significant differences in FeT/Al but Fe_{HR}/FeT is significantly lower in all three HS turbidite suites, in contrast to the BTB samples where the Fe_{HR}/FeT is always higher than in the Paleozoic database.

Framboid Size Distributions

The framboid size data for the graptolitic shale B1 below the Trilobite Bed show a typical log-normal distribution (see later) but the data from the remaining BTB and HS turbidite samples (figs. 2 and 3) show unusual features: the smallest framboids (< 5 µm) either are absent (or very rare), or they are a minor component of a bimodal population dominated by larger framboids. The smallest framboids are missing from the BTB pyritiferous turbidites (< 3 µm in B/109 and < 4.5 µm in B/103) and the HS host turbidites (H1 has one framboid at 3 µm, otherwise there are no framboids < 5 µm; H2 has one framboid at 3 µm, otherwise no framboids < 4.5 µm). The very smallest framboids (< 1µm diameter) are often absent but it is rare to have none in the

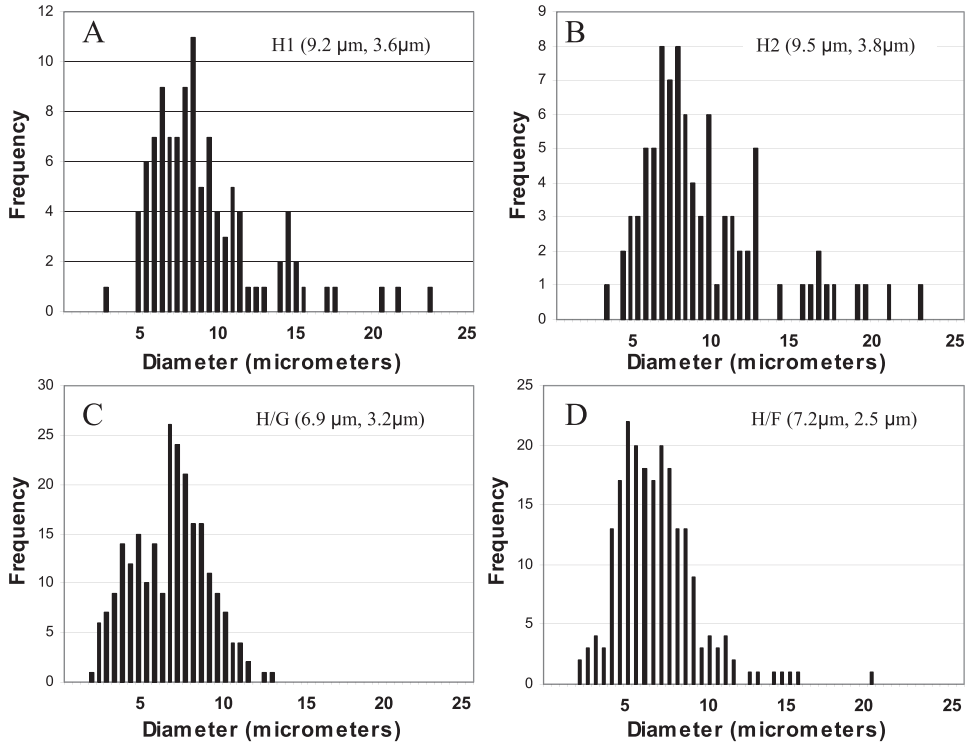

Fig. 3. Framboid size distributions in the Hunsrück Slate. (A) Host turbidite H1. (B) Host turbidite H2. (C) Pyritiferous turbidite H/G. (D) Pyritiferous turbidite H/F.

3 and 4 μm fractions (see the distributions in Wilkin and others, 1996, 1997; Wignall and Newton, 1998). The framboid sediment database in table 2 shows that all 104 samples contain framboids of 3 μm diameter, and all but 9 contain 2.5 μm framboids. The absence of small framboids is clearly rare.

The remaining turbidites (B2, H/G and H/F) show bimodal framboid distributions (figs. 2 and 3), with a minor but well-developed mode at smaller diameters. The B2 turbidite has a minor small diameter population with a maximum ~ 3 μm, the pyritiferous turbidite H/F has a minor small diameter population with a maximum at ~ 4 μm, and H/G has a more prominent small diameter population with a maximum ~ 5.5 μm.

Logarithmic probability plots (figs. 4 and 5) show that the B1 graptolitic shale data closely approximate a straight line over the 0 to 10 μm range; only occasional larger framboids depart from the log-normal distribution. The turbidite samples B2, H/G and H/F, on the other hand, show deviations from a log-normal distribution over the 0 to 10 μm range. In the case of H/G and H/F the deviations are sufficiently large to be resolved into intersecting straight lines corresponding to two main populations with means and standard deviations estimated as: H/G 8.5 ± 1.4 μm and 4.6 ± 1.2 μm; H/F 8.8 ± 2.2 μm and 5.2 ± 0.9 μm.

INTERPRETATION

Diagenetic Mineral Paragenesis

Two stages of diagenesis have been observed in re-sedimented turbiditic mudstones (Macquaker and others, 1997). A first stage of sulfate reduction formed

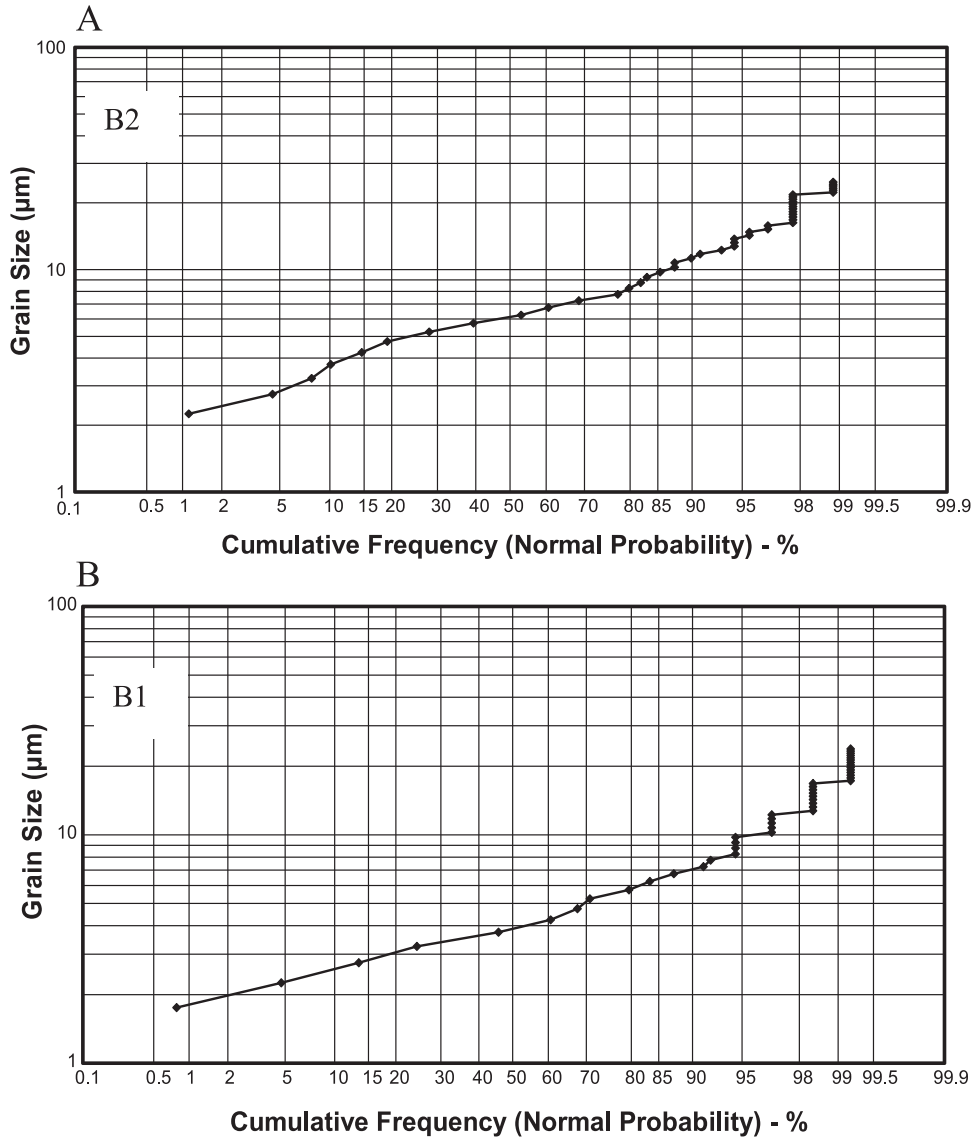

Fig. 4. Relationship between log (framboid diameter in µm) and cumulative frequency (on a probability scale) for Beecher's Trilobite Bed. (A) Pyritiferous turbidite B2. (B) Host sediment B1.

framboidal pyrite at the pre-transport site. Some of this pyrite survived transport to be deposited at the post-transport site where there was a renewed phase of sulfate reduction that produced additional framboidal pyrite. Thus the presence of bimodal framboid distributions and abraded aggregates of euhedral pyrite provide important insights into sulfide mineral paragenesis in BTB and the HS. Bimodality most probably arises from pyrite formation at both the pre-transport and post-transport sites.

There are two possible explanations for the loss of small framboids in BTB and the HS. Firstly, the smaller framboids may have been transported further and deposited in a more distal location and, secondly, framboids may have been lost by chemical

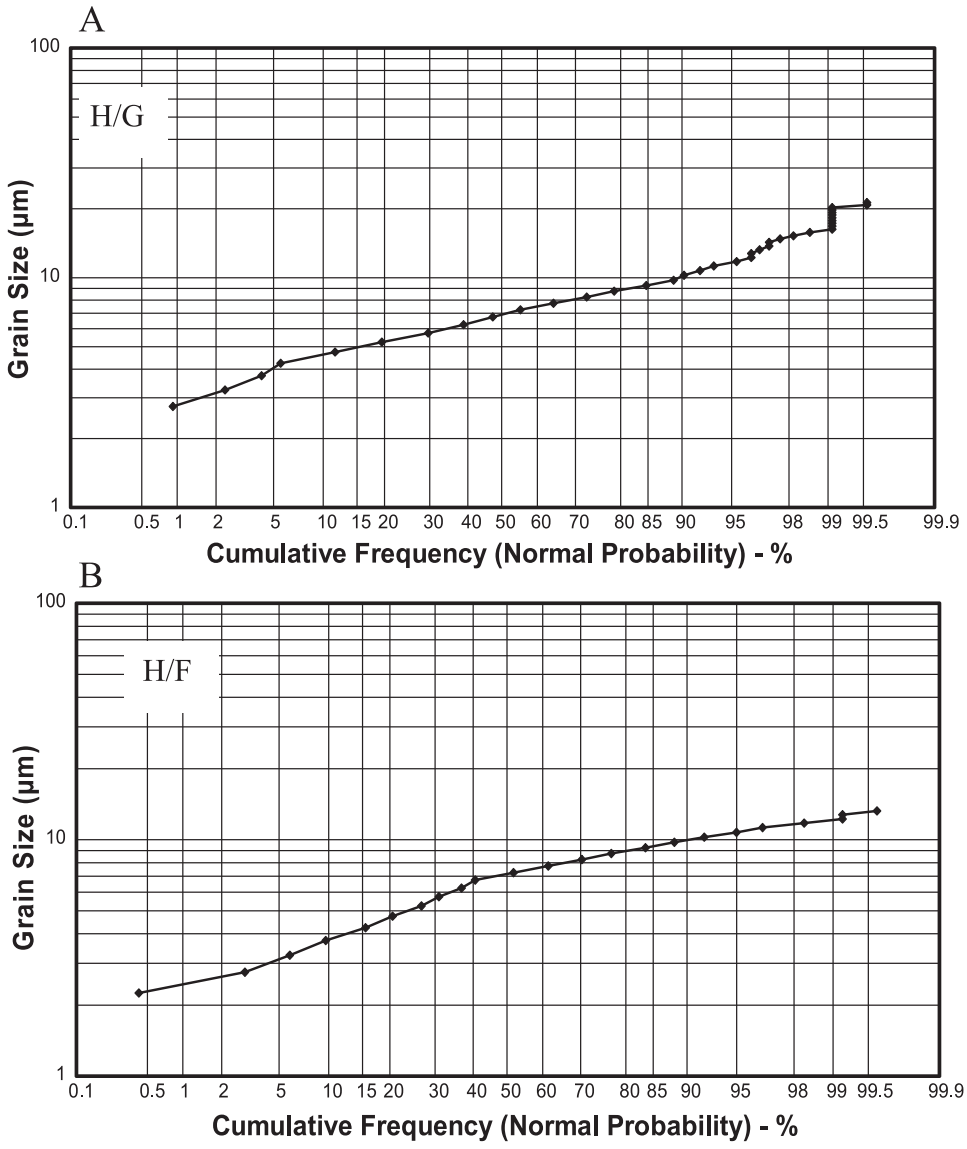

Fig. 5. Relationship between log (framboid diameter in µm) and cumulative frequency (on a probability scale) for the Hunsrück Slate. (A) Pyritiferous turbidite H/G. (B) Pyritiferous turbidite H/F.

oxidation due to exposure to oxygenated seawater during transport and burial. Both alternatives are possible for BTB and the HS. There is support for oxidation in the HS where the decalcification of aragonitic and calcitic fossils (Bartels and others, 1998) is generally associated with fossil pyritization (Tibbs, ms, 2001). Here oxidation of framboidal pyrite may have generated acids that produced carbonate undersaturation in the re-deposited sediments. Note that the loss of small framboids *alone* cannot account for the distributions observed in B2, H/G and H/F, which have two well-developed, reasonably symmetrical modes each with a clear maximum and conforming to log normality. The major and minor modes in these distributions appear to be

original, essentially unmodified, and are probably the result of the formation of one population at the pre-transport site and another at the post-transport site. Equally there is no evidence that the minor modes have been superimposed (to any significant extent) on a residual small diameter population from the pre-transport site. The simplest explanation of the framboid distributions in both BTB and the HS is that the turbidite samples lost a significant proportion of their smallest framboids during transport (by sorting or oxidation) but that, in some cases, post-transport diagenesis added a small diameter population. Metamorphism is an unlikely explanation for the loss of small framboids in the HS samples (H1 and H2) given the presence of well-defined small populations in H/G and H/F that pre-dated metamorphism.

Both phases of framboidal pyrite formed in an oxygenated environment, whereas euhedral pyrite formed later by direct precipitation from anoxic porewaters (Raiswell, 1982). Euhedral pyrite envelopes framboidal pyrite in both BTB and the HS. It is similar petrographically to that found in aggregate grains with eroded margins, indicating that at least some euhedral pyrite formed at the pre-transport site. It seems unlikely that all euhedral pyrite pre-dated transport but this possibility cannot be excluded. Thus the most probable sulfide mineral paragenesis in BTB and the HS is:1. Pre-transport framboidal pyrite; 2. Pre-transport euhedral pyrite; 3. Post-transport framboidal pyrite; 4. Post-transport euhedral pyrite.

Chemical Signatures

The Fe_{HR}/FeT ratios in both sets of samples from BTB are significantly higher than those in the Paleozoic sediment database, and the FeT/Al ratio is also significantly higher (but only at ~ the 10% level). This suggests that iron enrichment is more likely to reflect enhanced reactivity than addition. However the Fe_{HR} value of 1.2 percent in the pyritiferous turbidites (table 3) represents an addition of only 0.5 percent Fe_{HR} relative to the mean of ~0.7 percent in Paleozoic sediments (table 1). This increase in Fe_{HR} would have produced only a small change in FeT, from 4.93 percent to 5.43 percent, which is equivalent to a change in FeT/Al from 4.93/9.17 (or 0.54) to the current value of approximately 0.59 (which is only marginally significant; see above). The Fe_{HR}/FeT ratio is more sensitive to small changes in Fe_{HR} than the FeT/Al ratio, and clearly it is possible that a small addition of Fe_{HR} could have produced the observed changes in Fe_{HR}/FeT and FeT/Al. The chemical signatures therefore are consistent with iron enrichment either by addition and/or enhancement of reactivity. However the FeT/Al and Fe_{HR}/FeT ratios within the pyritiferous turbidites are not significantly different from those in the sediments above and below the Trilobite Bed, indicating that turbidite transport produced no measurable chemical changes.

FeT values are relatively high in the HS pyritiferous turbidites (compared to those in the other HS sample suites) but the similarity in the FeT/Al signatures in all three HS turbidites indicates that this difference is not due to the addition of highly reactive Fe but is the result of dilution by non-iron bearing phases. Consistent with this, none of the HS turbidites has an FeT/Al ratio that differs significantly from that in the Paleozoic sediments. All the HS samples are deposited from turbidites and therefore it is impossible to isolate the effects of turbidite deposition. However the similarity between the FeT/Al ratios of HS turbidites and the Paleozoic sediments suggests that no Fe enrichment was associated with turbidite deposition.

The lower values of Fe_{HR}/FeT and Fe_{PR}/FeT in the HS turbidites compared to the Paleozoic database most likely reflect the conversion of Fe_{HR} into Fe_{PR} and of Fe_{PR} into non-HCl soluble FeT during metamorphism. This decrease probably arose through late diagenesis and metamorphism when both highly and poorly reactive iron formed ankerite, iron-bearing chlorite and muscovite (phengite). These changes convert Fe_{HR} to Fe_{PR} and Fe_{PR} to non-HCl soluble FeT phases. In these circumstances the Fe_{HR}/FeT

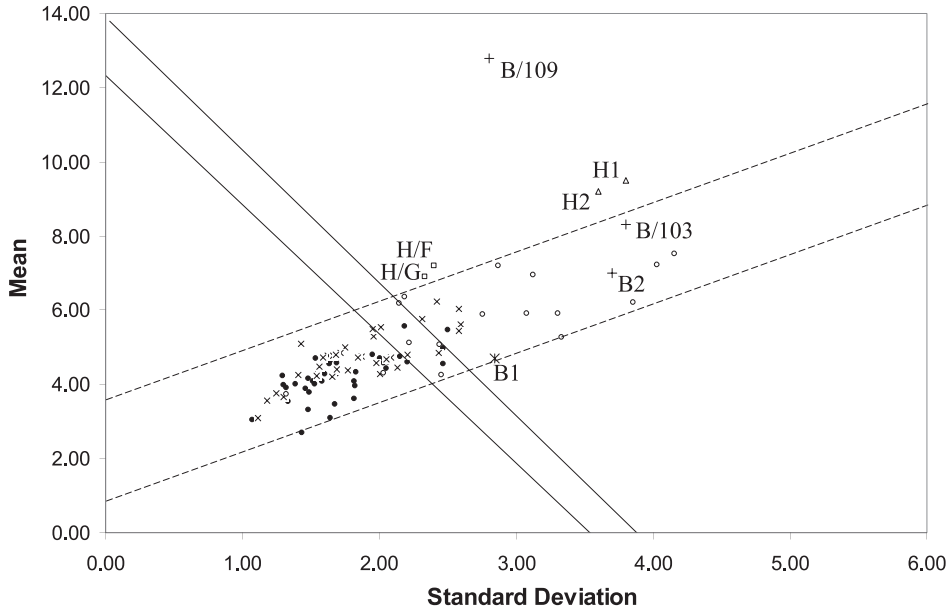

Fig. 6. Relationship between mean framboid diameter and population standard deviation (after Wilkin and others, 1996) for the framboids in table 2 (× ORB 1-2, ● ORB 3-4, ○ ORB 4.5-6 and oxic samples) and B/103, B/109, B2, B1, H/G, H/F, H1 and H2.

ratio is not a useful guide to Fe enrichment; the FeT/Al ratio provides a more reliable signature.

Framboid Size Distributions

Framboid size distributions provide paleoredox information because euxinic conditions produce framboids with a narrow size range (diameters < 5 μm) whereas sediments deposited from oxic and dysoxic bottom waters produce greater numbers of larger framboids and thus wider size distributions. These differences are presented in a plot (fig. 6) of mean framboid diameter against the standard deviation of the mean size (Wilkin and others, 1997). A line with the approximate equation

$$\text{Mean Size} = 12.5 - 2.9\ (\text{Std Dev}) \quad (1)$$

provides a good separation between a lower group of anoxic and an upper group of dysoxic (plus oxic) modern sediments for the data provided by Wilkin and others (1996), with only one modern oxic sample misclassified in the anoxic field. This line and a lower line with the same slope

$$\text{Mean Size} = 11 - 2.9\ (\text{Std. Dev}) \quad (2)$$

define a field that includes this oxic sample and two modern euxinic samples. Most of the ancient sediment framboid data presented in table 2 are also well-separated by the line represented by equation 1, which distinguishes an upper oxic/dysoxic field (with ORB 4.5−6 plus oxic samples) from a lower anoxic field (ORB 1 to 4). However one anoxic sample plots above this line and two oxic/dysoxic samples (ORB 4.5) plot below the line given by equation 2 which, nevertheless, represents the optimum separation. The field between lines given by equations 1 and 2 contains two anoxic and four oxic/dysoxic samples with ORB 4 and 4.5. Framboid size data in this field should

therefore be used with caution for paleoenvironmental interpretations. The ancient sediment data in table 2 otherwise fall in a broad band (represented by the dashed lines in fig. 6), as do the data of Wilkin and others (1996).

The BTB pyritiferous turbidites (B/103, B/109 and B2) plot in the oxic/dysoxic field of figure 6, clearly above the boundary represented by equation 1. The fossils were not transported far and the position of these BTB samples is consistent with the depositional environment inferred by Cisne (1973) and Briggs and others (1991). Nonetheless the diversity and paleoecology of the fauna indicates ORB 4, that is upper dysaerobic (Wignall, 1994). The framboid size distributions from the HS turbidites all plot in the oxic/dysoxic field, which is also consistent with both the inferred pre- and post-transport depositional environments. The pre-transport site for the Hunsrück Slate was a shallow (and presumably well-oxygenated) shelf and although the post-transport site has been interpreted as dysoxic (Brett and Seilacher, 1991) the diverse fauna indicates that it was well-oxygenated (Sutcliffe and others, 1999) above the sediment-water interface. Both post-transport bottom water conditions should produce framboid plots lying above the boundary given by equation 1. However, the HS turbidites also plot at varying distances above the diagonal band that includes all the ancient sediment data in table 2. Samples H1 and H2 clearly plot above the band due to relatively large mean diameters that arise from the absence of small framboids (see earlier). Samples H/G and H/F plot closer to the band because subdued small diameter populations occur in their bimodal distributions. However the resolved populations of the pyritiferous turbidites (H/G and H/F) are not wholly consistent with these bottom water conditions, as both of the larger populations plot in the oxic/dysoxic field and both of the smaller populations plot in the anoxic field. The size and standard deviation data derived from the resolved straight lines in figure 5 assume little overlap of the size populations. In practice a few large framboids that formed along with the smaller-size populations would increase the mean and standard deviation and displace these small, resolved populations into the oxic/dysoxic field in figure 6.

SYNTHESIS AND CONCLUSIONS

The pyritization of soft tissue results from two critical factors (Raiswell and others, 1993). First, the burial of soft tissue that is more readily metabolizable than organic matter in the surrounding sediments produces a site of rapid, localized sulfate reduction. Second, high dissolved iron concentrations in the surrounding sediments prevent the diffusive loss of sulphide and promote efficient precipitation of iron sulfide at the decay site. The evidence from chemical signatures, framboid size distributions and petrography can be integrated in their sedimentological context to suggest a sequence of events that produced these factors:

1. Anoxic conditions in the near-surface sediments at the pre-transport site allowed rapid sulfate reduction to form framboidal pyrite, where oxygen was available. Rates of sulfate reduction slowed down as the most readily metabolizable organic C was consumed. Euhedral pyrite was then formed by the direct precipitation of dissolved iron and sulfide under anoxic conditions. This sequence of events is unambiguous petrographically and firmly based on observations of pyrite formation in modern and ancient sediments (Berner, 1970, 1984; Goldhaber and Kaplan, 1974; Raiswell, 1982).
2. These near-surface sediments were mobilized by a turbidity current, which also enveloped benthic organisms. Aggregates of euhedral pyrite were abraded during transport. The fine-grained, abraded material, and the smallest framboids, were lost by size sorting or were oxidized as a result of mixing with oxygenated seawater, and the iron precipitated as (oxyhydr)oxides.

The FeT/Al and Fe_{HR}/FeT ratios of all the BTB samples are higher than in the Paleozoic sediment database but there is no significant difference between the Trilobite Bed and the host sediments. Hence turbidite deposition produced no enhancement of highly reactive Fe in the BTB. Enrichments relative to Paleozoic sediments in general must therefore be a provenance effect. The FeT/Al ratios of all the turbidite samples in the HS are not significantly different to that in the Paleozoic sediments in general, indicating that turbidite processes in the HS were not responsible for enrichment in highly reactive Fe. None of the FeT/Al chemical signatures indicate a loss of Fe_{HR}. Sediment Fe_{HR} contents would be conserved when framboids were oxidized and the iron re-precipitated as iron (oxyhydr)oxides, but would decrease if framboids were removed by sorting. These data suggest that the loss of the smallest framboids is probably a result of oxidation during transport and deposition. The smallest framboids in the HS may have been dissolved during metamorphism (see Wagner and Boyce, 2006) but this would not account for their absence from BTB.

Removal of the smallest framboids produces populations with a larger mean diameter and a smaller standard deviation, so that the B/103, B/109, H1 and H2 data plot above the diagonal band (fig. 6) that includes the other modern and ancient oxic/dysoxic sediments. Removal of framboids by oxidation would have enabled turbidite processes to deliver highly reactive iron to the porewater at a critical time to facilitate soft tissue pyritization.

3. The sediment was re-deposited as a turbidite. The residual, diminished stock of readily metabolizable organic C was sufficient only to produce suboxic conditions that favored iron reduction over sulfate reduction. Limited sulfate reduction produced framboidal pyrite (oxidants available from bioturbation) but porewaters contain dissolved iron in excess of dissolved sulfide.

Iron reduction in the turbidite was favored and sulfate reduction suppressed by low concentrations of readily metabolizable organic C (for example, Froelich and others, 1979; Aller and others, 1986; Burdige, 1993). After transport, diagenesis of BTB and HS turbidites re-started with a stock of readily metabolizable organic C which had been depleted during pre-transport diagnesis. There was also further depletion during post-transport oxic and suboxic diagenesis (involving O_2, NO_3^- and Mn) before iron reduction and sulfate reduction began. The oxidation of pre-transport framboidal pyrite produced fresh iron (oxyhydr)oxides that could be degraded readily by iron reduction (for example, Hyacinthe and Van Capellen, 2004).

4. The sediment conditions were now ideal for soft tissue pyritization. There was a sharp contrast between the enclosing sediments and the soft tissue of the buried organisms. Sulfate reduction was suppressed in the sediments by lack of metabolizable organic C while iron reduction maintained high concentrations of dissolved iron sourced from fresh iron (oxyhydr)oxides). The buried organisms, on the other hand, constituted a new source of readily metabolizable organic matter that could be degraded by sulfate reduction to produce H_2S. High concentrations of dissolved iron in the surrounding porewaters confined iron sulfide precipitation to the decaying soft tissue.

Ankerite formation in the HS most likely occurred at the end of this stage and is clear evidence for the existence of iron-bearing porewaters in the surrounding sediments. Oxygen was no longer available and slow rates of sulfate reduction in these sediments produced sulfide that was directly precipitated as euhedral pyrite.

In conclusion, the use of physical and chemical signatures provides a valuable insight into diagenetic processes in BTB and the HS which resulted in conditions that facilitated soft tissue pyritization. The framboid size distributions record, for the first time, how transport and post-transport processes influenced sediment and porewater compositions. Consistent with this, the intra-basinal chemical signatures clearly show

that turbidite depositional processes did not enrich iron in the BTB or HS sediments. Comparison with a Paleozoic sediment database confirms that the BTB sediments are all enriched in highly reactive iron (as concluded by Briggs and others, 1991). However, the intra-basinal comparison shows that this enrichment, which may have helped create conditions suitable for soft tissue pyritization, is a source area effect that pre-dated transport. The use of the Paleozoic sediment database thus provides a useful threshold for the recognition of iron enrichment on a global scale.

ACKNOWLEDGMENTS

This study was funded by a NERC research award (GR3/11966) to RR and SHB, including a studentship (GT 16/99/ES/17) to PMC. We are grateful to the owners of the Beecher's Bed Quarry for allowing access, and to them and Tom Whiteley for greatly facilitating our research at the locality. Our work on the Hunsrück Slate would not have been possible without the generous assistance and advice of Dr. Christoph Bartels. Dan Parsons produced the programme to draw the log. grain size /probability plots. We also thank the owners of Schiefergrübe Eschenbach-Bocksberg, Johann and Backes, for access and help in obtaining Hunsrück Slate samples. We are grateful for discussion with Una Farrell and for comments from Robert Gaines, Joe Macquaker and Tim Lyons. This is Project *Nahecaris* contribution number 25.

References

Aller, R. C., Mackin, J. E., and Cox, R. T., Jr., 1986, Diagenesis of Fe and S in Amazon inner shelf muds: apparent dominance of Fe reduction and implications for the genesis of ironstones: Continental Shelf Research, v. 6, p. 263–289.

Anderson, T. F., and Raiswell, R., 2004, Sources and mechanisms for the enrichment of highly reactive iron in euxinic Black Sea sediments: American Journal of Science, v. 304, p. 203–233.

Aplin, A. C., and Macquaker, J. H. S., 1993, C-S-Fe geochemistry of some modern and ancient anoxic muds and mudstones: London, Philosophical Transactions of the Royal Society, v. 344A, p. 89–100.

Bartels, C., and Brassel. G., 1990, Fossilien im Hunsruckschiefer-Dokumente des Meereslebens im Devon: Idar-Oberstein, Museum Idar-Oberstein, 232 p.

Bartels, C., Briggs, D. E. G., and Brassel, G., 1998, The fossils of the Hunsrück Slate: Marine life in the Devonian: Cambridge, Cambridge University Press, 309 p.

Bartels, C., Wuttke, M., and Briggs, D. E. G., 2002a, The *Nahecaris* project: releasing the marine life of the Devonian from the Hunsrück Slate of Bundenbach (SW Germany). Preliminary results and unresolved questions: Metalla, v. 9, p. 59–72.

Bartels, C., Poschmann, M., Schindler, T., and Wuttke, M., 2002b, Palaeontology and palaeoecology of the Kaub Formation (Lower Emsian, Lower Devonian) at Bundenbach (Hunsrück, SW Germany): Metalla, v. 9, p. 105–122.

Berner, R. A., 1970, Sedimentary pyrite formation: American Journal of Science, v. 267, p. 19–42.

——— 1984, Sedimentary pyrite formation; an update: Geochimica et Cosmochimica Acta, v. 48, p. 605–615.

Bond, D. P. G., ms, 2004, Oceanographic Changes during the Late Frasnian-Famennian Mass Extinction: Leeds, United Kingdom, University of Leeds, Ph. D. Thesis, 289 p.

Brett, C. E., and Seilacher, A., 1991, Fossil Lagerstätten; a taphonomic consequence of event sedimentation, *in* Einsele, G., Ricken, W., and Seilacher, A., editors, Cycles and Events in Stratigraphy: Berlin, Springer-Verlag, p. 283–297.

Briggs, D. E. G., and Edgecombe, G. D., 1993, Beecher's Trilobite Bed: Geology Today, v. 9, p. 97–102.

Briggs, D. E. G., Bottrell, S. H., and Raiswell, R., 1991, Pyritization of soft bodied fossils: Beechers Trilobite Bed, Upper Ordovician, New York State: Geology, v. 19, p. 1221–1224.

Briggs, D. E. G., Raiswell, R., Bottrell, S. H., Hatfield, D., and Bartels, C., 1996, Controls on the pyritization of exceptionally well preserved fossils: An analysis of Lower Devonian Hunsrück Slate of Germany: American Journal of Science, v. 295, p. 633–663.

Burdige, D. J., 1993, The biogeochemistry of manganese and iron reduction in marine sediments: Earth Science Reviews, v. 35, p. 249–284.

Calvert, S. E., Thode, H. G., Young, D., and Karlin, R. E., 1996, A stable isotope study of pyrite formation in the Late Pleistocene and Holocene sediments of the Black Sea: Geochimica et Cosmochimica Acta, v. 60, p. 1261–1270.

Canfield, D. E., 1989, Reactive iron in marine sediments: Geochimica et Cosmochimica Acta, v. 3, p. 619–632.

Canfield, D. E., and Raiswell, R., 1991, Pyrite Formation and Fossil Preservation, *in* Allison, P. A., and Briggs, D. E. G., editors, Taphonomy: Releasing the Data Locked in the Fossil Record: New York, Plenum, p. 337–387.

Canfield, D. E., Raiswell, R., and Bottrell, S. H., 1992, The reactivity of sedimentary iron minerals towards sulfide: American Journal of Science, v. 292, p. 659–683.

Canfield, D. E., Lyons, T. W., and Raiswell, R., 1996, A model for iron deposition to euxinic Black Sea sediments: American Journal of Science, v. 296, p. 818–834.
Cisne, J. L., 1973, Beecher's Trilobite Bed revisited: Ecology of an Ordovician deepwater fauna: Postilla, v. 160, 25 p.
Clarke, F. W., 1924, Data on Geochemistry: US Geological Survey Bulletin, v. 770.
Coburn, P. M., ms, 2003, A Sulphur Isotope and Geochemical Study of Soft Tissue Pyritisation in Shales: Leeds, United Kingdom, University of Leeds, Ph. D. Thesis, 289 p.
Deflandre, B., Mucci, A., Gagne, J. P, Guignard, C., and Sundby, B., 2002, Early diagenetic processes in coastal marine sediments disturbed by a catastrophic sedimentation event: Geochimica et Cosmochimica Acta, v. 66, p. 2547–2558.
Formolo, M. J., and Lyons, T. W., 2007, Accumulation and preservation of reworked marine pyrite beneath an oxygen-rich Devonian atmosphere: Constraints from sulfur isotopes and framboid textures: Journal of Sedimentary Research, v. 77, p. 623–633.
Fortey, R., 2000, Olenid trilobites: the oldest known chemoautotrophic symbionts?: Proceedings of the National Academy of Sciences, v. 97, p. 6574–6578.
Froelich, P. N., Klinkhammer, G. P., Bender, M. L., Luedtke, N. A., Heath, G. R., Cullen, D., Dauphin, P., Hammond, D., Hartman, D., and Maynard, V., 1979, Early oxidation of organic matter in pelagic sediments of the eastern equatorial Atlantic: suboxic diagenesis: Geochimica et Cosmochimica Acta, v. 43, p. 1075–1090.
Garrels, R. M., and Mackenzie, F. T., 1971, Evolution of Sedimentary Rocks: New York, Norton, 397 p.
Goldhaber, M. B., and Kaplan, I. R., 1974, The sulfur cycle, *in* Goldberg, E. D., editor, The Sea, v. 5: New York, Wiley-Interscience, p. 560–655.
Graham, U. M., and Ohmoto, H., 1994, Experimental study of formation mechanisms of hydrothermal pyrite: Geochimica et Cosmochimica Acta, v. 58, p. 2187–2202.
Hunger, S., and Benning, L. G., 2007, Greigite: a true intermediate on the polysulfide pathway to pyrite: Geochemical Transactions, v. 8 :1, doi:10.1186/1467-4866-8-1.
Hyancinthe, C., and Van Capellen, P., 2004, An authigenic iron phosphate phase in estuarine sediments: Composition, formation and chemical reactivity: Marine Chemistry, v. 91, p. 227–251.
Koch, G. S., and Link, R. F., 1971, Statistical Analysis of Geological Data, v. 2: New York, Wiley and Sons, 438 p.
Love, L. G., and Amstutz, G. C., 1966, Review of microscopic pyrite from the Chattanooga Shale and Rammelsberg Banderz: Fortschritte der Mineralogie, v. 43, p. 273–309.
Luther, G. W., III, 1991, Pyrite synthesis via polysulfide compounds: Geochimica et Cosmochimica Acta, v. 55, p. 2839–2849.
Lyons, T. W., 1997, Sulfur isotopic trends and pathways of iron sulfide formation in upper Holocene sediments of the anoxic Black Sea: Geochimica et Cosmochimica Acta, v. 61, p. 3367–3382.
Lyons, T. W., and Severmann, S., 2006, A critical look at iron paleoredox proxies based on new insights from modern euxinic marine basins: Geochmica et Cosmochimica Acta, v. 70, p. 5698–5722.
Lyons, T. W., Werne, J. P., Hollander, D. J., and Murray, R. W., 2003, Contrasting sulfur geochemistry and Fe/Al and Mo/Al ratios across the last oxic-to-anoxic transition in The Cariaco Basin, Venezuela: Chemical Geology, v. 195, p. 131–157.
Macquaker, J. H. S., Curtis, C. D., and Coleman, M. L., 1997, The role of iron in mudstone diagenesis: Comparison of Kimmeridge Clay Formation mudstones from onshore and offshore (UKCS) localities: Journal of Sedimentary Research, v. 67, p. 871–878.
Massad, M., 1974, Framboidal pyrite in concretions: Mineralia Deposita, v. 9, p. 87–89.
Mucci, A., and Edenborn, H. M., 1992, Influence of an organic-poor landslide deposit on the early diagenesis of iron and manganese in a coastal marine sediment: Geochimica et Cosmochimica Acta, v. 56, p. 3909–3921.
Muramoto, J. A., Honjo, S., Fry, B., Howarth, R. W., and Cisne, J. L., 1991, Sulfur, iron and organic carbon fluxes in the Black Sea: Sulfur isotopic evidence for origin of sulfur fluxes: Deep-Sea Research, v. 38, p. 1151–1187.
Newton, R. J., ms, 2001, The Characterization of Depositional Environments using Fe, S and C Geochemistry: Leeds, United Kingdom, University of Leeds, Ph. D. thesis, 206 p.
Ohfuji, H., and Rickard, D., 2005, Experimental sytheses of framboids- a review: Earth Science Reviews, v. 71, p. 147–170.
Papunen, H., 1966, Framboidal texture of the pyritic layer found in a peat bog in SE Finland: Bulletin de la Commission Geologique de Finlande, v. 222, p. 117–125.
Poulton, S. W., and Raiswell, R., 2002, The low temperature geochemical cycle of iron; From continental fluxes to marine sediment deposition: American Journal of Science, v. 302, p. 774–805.
——— 2005, Chemical and physical characteristics of iron oxides in riverine and glacial meltwater sediments: Chemical Geology, v. 218, p. 203–221.
Poulton, S. W., Krom, M. D., and Raiswell, R., 2004, A revised scheme for the reactivity of iron (oxyhydr)oxide minerals towards dissolved sulfide: Geochimica et Cosmochimica Acta, v. 68, p. 3703–3715.
Raiswell, R., 1982, Pyrite texture, isotopic composition and the availability of iron: American Journal of Science, v. 282, p. 1244–1263.
Raiswell, R., and Anderson, T. F., 2005, Reactive iron enrichment in sediments deposited beneath euxinic bottom waters: Constraints on supply by shelf recycling, *in* McDonald, I., Boyce, A., Butler, I. B., Herrington, R. J., and Polya, D. A., editors, Mineral Deposits and Earth Evolution: London, Geological Society Special Publication, v. 248, p. 179–194.

Raiswell, R., and Berner, R. A., 1986, Pyrite and organic matter in Phanerozoic normal marine shales: Geochimica et Cosmochimica Acta, v. 60, p. 1967–1976.
Raiswell, R., and Canfield, D. E., 1996, Rates of reaction between silicate iron and dissolved sulfide in Peru Margin sediments: Geochmica et Cosmochimica Acta, v. 60, p. 2777–2787.
——— 1998, Sources of iron for pyrite formation: American Journal of Science, v. 298, p. 219–245.
Raiswell, R., Whaler, K., Dean, S., Coleman, M. L., and Briggs, D. E. G., 1993, A simple three-dimensional model of diffusion-with-precipitation applied to localised pyrite formation in framboids, fossils and detrital iron minerals: Marine Geology, v. 113, p. 89–100.
Raiswell, R., Canfield, D. E., and Berner, R. A., 1994, A comparison of iron extraction methods for the determination of degree of pyritisation and the recognition of iron-limited pyrite formation: Chemical Geology, v. 111, p. 101–111.
Raiswell, R., Newton, R., and Wignall, P. B., 2001, An indicator of water-column anoxia: resolution of biofacies variations in the Kimmeridge Clay (Upper Jurassic, U.K.): Journal of Sedimentary Research, v. 71, p. 286–294.
Rickard, D. T., 1970, The origin of framboids: Lithos, v. 3, p. 269–293.
——— 1975, Kinetics and mechanisms of pyrite formation at low temperatures: American Journal of Science, v. 275, p. 636–652.
——— 1997, Kinetics of pyrite formation by the H_2S oxidation of iron (II) monosulfide in aqueous solutions between 25°C and 125°C: the rate equation: Geochimica et Cosmochimica Acta, v. 61, p. 115–134.
Rickard, D. T., and Luther, G. W., III, 2007, Chemistry of iron sulfides: Chemical Reviews, v. 107, p. 514–562.
Ronov, A. B., and Migdisov, A. A., 1971, Geochemical history of crystalline basement and sedimentary cover of the Russian and North American Platforms: Sedimentology, v. 16, p. 173–183.
Roy, A. S., 1978, Evolution of slaty cleavage in relation to diagenesis and metamporphism: a study from the Hunsrückschiefer: Geological Society of America Bulletin, v. 89, p. 1773–1785.
Sawlowicz, Z., 1993, Pyrite framboids and their development; a new conceptual mechanism: Geologische Rundschau, v. 82, p. 148–156.
Schoonen, M. A. A., and Barnes, H. L., 1991, Reactions forming pyrite and marcasite from solution: Geochimica et Cosmochimica Acta, v. 55, p. 1505–1514.
Sinclair, A. J., 1974, Selection of threshold values in geochemical data using probability graphs: Journal of Geochemical Exploration, v. 3, p. 129–149.
Sutcliffe, O. E., Briggs, D. E. G., and Bartels, C., 1999, Ichnological evidence for the environmental setting of the Fossil-Lagerstätten in the Devonian Hunsrück slate, Germany: Geology, v. 27, p. 275–278.
Sutcliffe, O. E., Tibbs, S. L., and Briggs, D. E. G., 2002, Sedimentology and environmental interpretation of fine-grained turbidites in the Kaub Formation of the Hunsrück Slate: analysis of a section excavated for Project Nahecaris: Metalla, v. 9, p. 89–104.
Talbot, J. L., 1964, Crenulation cleavage in the Hunsrückschiefer of the Middle Mosell region: Geologische Rundschau, v. 54, p. 1026–1043.
Taylor, S. R., and McLennan, S. M., 1985, The Continental Crust: Its Composition and Evolution: Oxford, Blackwell Scientific Publications, 328 p.
Tibbs, S. L., ms, 2001. Mineralisation of Fossils from the Lower Devonian Hunsrück Slate, Germany: Bristol, United Kingdom, University of Bristol, Ph. D. Thesis, 341 p.
Wagner, T., and Boyce, A. J., 2006, Pyrite metamorphism in the Devonian Hunsruck Slate of Germany: Insights from laser sulfur isotope analysis and thermodynamic modeling: American Journal of Science, v. 306, p. 525–552.
Werne, J. P., Sageman, B. B., Lyons, T. W., and Hollander, D. J., 2002, An integrated assessment of a type 'euxinic' deposit: Evidence for multiple controls on black shale deposition in the Middle Devonian Oatka Creek Formation: American Journal of Science, v. 302, p. 110–143.
Wignall, P. B., 1994, Black Shales: Oxford, Clarendon Press, 127 p.
Wignall, P. B., and Hallam, A., 1991, Biofacies, stratigraphic distribution and depositional models of British onshore Jurassic Black shales, *in* Tyson, R. V., and Pearson, T. H., editors, Modern and Ancient Continental Shelf Anoxia: London, Geological Society Special Publication, v. 58, p. 291–309.
Wignall, P. B., and Newton, R. J., 1998, Pyrite framboid diameter as a measure of oxygen deficiency in ancient mudrocks: American Journal of Science, v. 298, p. 537–552.
Wijsman, J. W. M., Middleburg, J. J., and Heip, C. H. R., 2001, Reactive iron in Black Sea sediments: implications for iron cycling: Marine Geology, v. 172, p. 167–180.
Wilkin, R. T., and Arthur, M. A., 2001, Variations in pyrite texture, sulfur isotope composition, and iron systematics in the Black Sea: Evidence for Late Pleistocene to Holocene excursions of the O_2-H_2S redox transition: Geochimica et Cosmochimica Acta, v. 65, p. 1399–1416.
Wilkin, R. T., and Barnes, H. L., 1997, Formation processes of framboidal pyrite: Geochimica et Cosmochimica Acta, v. 61, p. 323-339.
Wilkin, R. T., Barnes, H. L., and Brantley, S. L., 1996, The size distribution of framboidal pyrite in modern sediments: An indicator of redox conditions: Geochimica et Cosmochimica Acta, v. 60, p. 3897–3912.
Wilkin, R. T., Arthur, M. A., and Dean, W. E., 1997, History of water column anoxia in the Black Sea indicated by pyrite framboid size distributions: Earth and Planetary Science Letters, v. 148, p. 517–525.
Wilson, T. R. S., Thomson, J., Colley, S., Hydes, D. J., Higgs, N. C., and Sorenson, J., 1985, Early organic diagenesis: The significance of progressive subsurface oxidation fronts in pelagic sediments: Geochimica et Cosmochimica Acta, v. 49, p. 811–822.
Wilson, T. R. S., Thomson, J., Hydes, D. J., Colley, S., Culkin, F., and Sorenson, J., 1986, Oxidation fronts in pelagic sediments: Diagenetic formation of metal-rich layers: Science, v. 232, p. 972–975.